Separation and Purification Technology 67 (2009) 355–363

Contents lists available at ScienceDirect

Separation and Purification Technology

journal homepage: www.elsevier.com/locate/seppur

Optimisation of an annular photoreactor process for degradation of Congo Red using a newly synthesized titania impregnated kaolinite nano-photocatalyst

Meng Nan Chong[a,b], Shaomin Lei[c], Bo Jin[a,b,d,*], Chris Saint[b,d], Christopher W.K. Chow[d]

[a] School of Chemical Engineering, The University of Adelaide, Adelaide, SA 5000, Australia
[b] School of Earth and Environmental Sciences, The University of Adelaide, Adelaide, SA 5000, Australia
[c] School of Resource and Environment Engineering, Wuhan University of Technology, Wuhan 430070, China
[d] Australian Water Quality Centre, SA Water Corporation, Bolivar, SA 5110, Australia

ARTICLE INFO

Article history:
Received 3 June 2008
Received in revised form 31 March 2009
Accepted 2 April 2009

Keywords:
Photocatalysis
TiO_2
Congo Red
Kaolinite
Annular reactor
Degradation

ABSTRACT

In this study, an annular photocatalytic reactor (APR) system was designed and operated to optimise the photocatalytic degradation of Congo Red (CR) using a newly synthesized titania impregnated kaolinite photocatalyst (TiO_2/K). The design parameters of the APR: reactor configuration, mass transfer, mixing and hydrodynamics were discussed. The influences of the operation parameters: pH, critical TiO_2/K loading, aeration rate and initial CR concentration on the photocatalytic performances were studied in a batch operation mode. Results showed that the initial pH was the most crucial operation parameter that significantly affected both the adsorption and photocatalytic reactions in the APR–TiO_2/K system. The point of zero charge for TiO_2/K was found to shift towards pH 9.5. The complete degradation of 40 ppm CR was attained in 4 h. Possible intermediates and by-products during the CR degradation were identified using the LC/MS technique. The TiO_2/K reactivation study showed that the TiO_2/K particles are highly stable and have a modest improvement in photoactivity for every recycle trial up to at least five cycles. The overall results revealed that the APR–TiO_2/K system has promising application for the development of a technically feasible and cost-effective industrial water and wastewater treatment process.

1. Introduction

Water treatment utilising semiconductor titanium dioxide (TiO_2) has been the centre of research owing to its high photocatalytic efficiency in degrading a wide range of organic contaminants [1–8]. When the TiO_2 particle absorbs a photon with energy greater than the band gap energy ($E_b \geq 3.2$ eV), the lone electron in the valence band will be excited to the conduction band and thus creating the electron–hole pair [9–11]. Whilst the electron–hole pair remains separated, the valence band hole will oxidise the hydroxyl groups that are present in the aqueous environment to the highly oxidative hydroxyl radicals (•OH) [8–10]. Simultaneously, the conduction band electron will capture the electron scavengers (e.g. dissolved oxygen) creating the superoxide radical (•O) [5,6,9,10]. It was reported that only incomplete mineralisation of s-triazines was examined in the non-aqueous solvents [9]. Thus the presence of water molecules plays an important role in an effective photocatalysis process.

The mechanism for the generation of an electron–hole pair depicted that TiO_2 photocatalysis is a surface-oriented reaction [12]. The main oxidation process for the organic compounds in an aqueous environment takes place on the surface of the TiO_2 particles. Herrmann [9] proposed that the heterogeneous photocatalysis can be proceeded in five independent steps. Initially the transferred organic compounds will adsorb onto the photon activated TiO_2 surface, proceeding with the surface reaction and desorption of the intermediates or final photodegradation by-products and finally the removal of these by-products from the interface region. This indicates that the photocatalysis process is mass transfer limiting and further efforts should be emphasized in the development of appropriate photocatalytic reactor system.

Two common types of photo-reactors: a slurry reactor or a fixed bed reactor, were usually used in the previous investigations [13,14]. The fixed bed reactor has the advantage in downstream separation after water treatment [17–19]. However, there are a number of key issues associated with the application of a fixed bed reactor that need further consideration, including poor mass transfer, severe light attenuation over the coated TiO_2 film, decrease in specific surface area for reaction and the increasing difficulties in photocatalyst reactivation and reuse [14,17]. Ideally the slurry reactor would be the most suitable photo-oxidation system due to its large

* Corresponding author at: School of Earth and Environmental Sciences, The University of Adelaide, Adelaide, SA 5005, Australia. Tel.: +61 8 8303 7056; fax: +61 8 8303 6222.
E-mail address: bo.jin@adelaide.edu.au (B. Jin).

1383-5866/$ – see front matter © 2009 Elsevier B.V. All rights reserved.
doi:10.1016/j.seppur.2009.04.001

Nomenclature

APR	annular photocatalytic reactor
C	concentration at time, t (ppm or mg/dm^3)
C_0	initial concentration (ppm or mg/dm^3)
COD	chemical oxygen demand
C_μ	viscosity correction factor
CR	Congo Red
DO	dissolved oxygen
d_T	diameter of the reactor (cm)
E_b	bandgap energy
k	reaction rate constant, k (min^{-1})
K	kaolinite
LC/MS	liquid chromatograph/mass spectrometry
•O	superoxide radical
•OH	hydroxyl radical
PZC	point of zero charge
S_T	surface tension of liquid (dyne/cm)
t	irradiation time (h)
TiO_2	titanium dioxide
TiO_2/K	titania impregnated kaolinite
u_g	superficial gas velocity in the reactor (cm/s)
u_{tp}	terminal settling velocity of particles (cm/s)
UV	ultraviolet light
W_{max}	critical solid loading (g/cm^3)

Greek letters

γ	wettability factor
ε_g	gas holdup
ρ_G, ρ_L	density of gas and liquid respectively (g/cm^3)
μ_G, μ_L	viscosity of gas and liquid phases respectively (g/cm/s)

reaction surface area in the reactor, leading to high oxidation and degradation efficiency [14,15]. However, the efficient application of a slurry reactor should be coupled with a photocatalyst or a separation unit that permits ease of separation after the photocatalytic reaction [12,15,16]. Recovery of the photocatalysts for the reactor system is one of a few technical challenges associated with the application of the slurry reactor for water/wastewater treatment.

In this study, a newly synthesized titania impregnated kaolinite (TiO_2/K) nano-photocatalyst was utilised for the photocatalytic degradation of Congo Red (CR) in an newly designed annular photocatalytic reactor (APR) system. The application of TiO_2/K was expected to take full advantage of the enhanced adsorption, structurally rigid and separable properties provided by kaolinite (K) particles, while maintaining a high specific surface area for enhanced mass transfer and photocatalytic reaction. The influences of operational parameters: initial pH, TiO_2/K loading, aeration rate and initial CR concentration will be optimised in the APR system. Degradation mechanisms will be assessed by chemical oxygen demand (COD) and possible intermediates formed during the CR degradation. For the first time, the reclaimed and subsequent reactivation of the slurry TiO_2/K photocatalyst was carried out in this study.

2. Materials and methods

2.1. Materials

Titanium (IV) butoxide (tetrabutyl orthotitanate, purum grade ≥97% gravimetric, Sigma–Aldrich) was used as received. Raw kaolinite (K) materials were obtained from Unimin, Australia. Congo Red ($C_{32}H_{22}N_6Na_2O_6S_2$, Labchem Ajax Finechem, Australia) was prepared to a designated concentration by the addition of Milli-Q.

2.2. Preparation of titania impregnated kaolinite (TiO_2/K) photocatalyst

The preparation of TiO_2/K nano-photocatalyst has been reported in our previous study [20]. The TiO_2/K photocatalyst is synthesized via a modified two-step sol–gel method. In the first step, 25 mL of titanium (IV) butoxide was hydrolysed in 30 mL of absolute ethanol. The mixture was stirred for 30 min to allow homogenous mixing and the resultant hydrolysed mixture was denoted as mixture A. Then the mixture A was slowly mixed into 0.28 M HNO_3 for the condensation reaction. The resultant mixture denoted as mixture B was stirred for 4 h. Concurrently a 10% (w/v) of pre-treated K suspension was prepared in a three-necked round bottom flask kept in a water bath at 37 °C. The K particles were pre-treated by sedimentation, filtration, base treatment and were finally outgassed at 750 °C for 1 h. The resultant mixture B was then added drop wise with the aid of a separatory funnel into the flask and then stirred rigorously with an overhead stirrer. Stirring of the contents in the three-necked flask (mixture C) was extended for 30 min after the total addition of mixture B. The resultant mixture C was then filtered and washed repeatedly with distilled water up to three times before being dried in a conventional oven at 65–70 °C for 3 h. The resultant filtrate cake was then brushed off from the filter paper into the crucibles and further subjected to calcination at 600 °C for 3 h.

2.3. Annular photocatalytic reactor system set-up

A self-designed APR with an interchangeable diameter of a quartz thimble was used in this study. The design of the reactor allowed the option of inserting additional UV lamps into the z-axis during the operation. The annular reactor was fabricated from stainless steel with a detachable conical bottom for ease of cleaning and scheduled maintenance. The quartz thimble located in the core axis of the reactor was used to protect the UV lamp from direct contact with the reaction fluid. The quartz thimble allows maximum UV transmission into the reaction zone without any impedance. The bottom portion of the reactor was conical to prevent the existence of a dead zone during the gas bubbling of the slurry TiO_2/K photocatalyst. A gas sparger was fitted to the detachable conical bottom, with an average pore size of 45 μm. There are four sampling ports hosted on the reactor. Three ports are located in an elevated row while the other port was an optional for base dosing purposes. The three elevated sampling ports on the same row allow for ease of sampling when the volume of the reaction fluid dropped during the experimental period. A cooling water jacket was fabricated at the top of the reactor in order to maintain or cool down the temperature if the UV light over-generated heat energy. An 11 W UV light (Davis Ultraviolet, Australia) that peaks at 256 nm was inserted between the quartz thimble during the experiment. The detailed design of the reactor and the experimental set-up for the APR system are sketched in Fig. 1. The APR system consists of the annular reactor, cooling water recirculation line, cooling water pump, water storage tank and compressed air line fitted with a regulator valve. The pH, dissolved oxygen (DO) and temperature probes and meters (TPS, Australia) were connected to the specially designed ports in the annular reactor. All the other fluid connection lines in the APR system were fitted in accordance to their diameter size by Tygon tubes.

2.4. Experimental set-up

Initially a stock solution with 40 mg/dm^3 of CR was prepared. The pH of the solution was adjusted using 2 M of hydrochloric acid

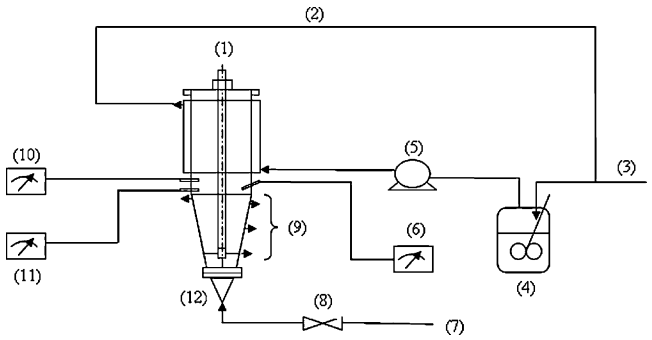

Fig. 1. Experimental set-up for the annular photocatalytic reactor system: (1) UV light, (2) recirculation water line, (3) fresh cool water line, (4) cooling water vessel, (5) cooling water pump, (6) temperature meter, (7) compressed air supply line, (8) compressed air regulation valve, (9) sampling ports, (10) pH meter, (11) dissolved oxygen meter, and (12) photoreactor.

(HCl) and sodium hydroxide (NaOH), respectively, as per experimental requirement. Using a correlation for the CR concentration with the UV–vis absorption spectra at 496.5 nm, a calibration curve was obtained by series dilution of the stock solution. Then the determined TiO_2/K loading for the experiment was measured. Prior to the introduction of the CR solution into the reactor, the reactor was aerated at a 0.5 dm^3/min. When the gas flowrate achieved steady state, both the CR solution and TiO_2/K was introduced into the reactor. The slurry mixture was mixed and aerated for 30 min before the UV lamp was turned on at $t = 0$ h. Sampling of the reaction fluid was then carried out for every hour from the three sampling ports. The samples were then centrifuged (Eppendorf Centrifuge 5415R, Germany) at 5000 rpm for 10 min. The supernatant was decanted and filtered using Millex VX filter (Millipore 0.45 μm) to ensure it was free of TiO_2/K particles. The filtered solution was then used to measure CR concentration by UV–vis spectrophotometer (Helios Gamma, England).

2.5. Analysis methods

Chemical oxygen demand (COD) for the samples was measured using a COD measurement kit (Hach, United States). The COD measurement kit comprises of the 0–150, 1500, 15000 ppm COD digestion solution, Hach DRB 200 digestion chamber and Hach DR890 COD calorimeter. Two milliliter of the filtered samples were added into the digestion solution. The digestion solution was then subjected to the digestion chamber at 70 °C for 120 min. After the digestion, the solution was allowed to cool down prior to the COD measurements using the calorimeter.

The degradation of CR and its intermediate products were verified using a liquid chromatograph/mass spectrometry (LC/MS). The LC separation was provided by a Waters liquid chromatograph (Waters, Milford USA), which consists of a 2695 Separation Module and 2487 dual wavelength UV detector. The operating conditions were as follows: HPLC column (SGE Wakosil 2 mm × 150 mm C18); ammonium acetate–acetonitrile; flow rate of 0.2 mL/min; injection volume of 20 μL; UV detector at 235 nm and 350 nm. The entire flow from LC was then directed into a Micromass Quattro micro tandem quadrupole MS (Waters, Manchester UK). Data were acquired by the Masslynx data system for both the MS and UV data. The MS analysis was operated in both positive and negative ion electrospray mass spectrometry (ESI). The operating conditions for one of the negative ion ESI was as follows; capillary of 3.5 kV; source temperature of 80 °C; desolvation temperature and gas flow of 350 °C and 500 L/h, respectively; scan duration of 1 s; mass range scanned of 80–800; cone of 30–70 V.

3. Results and discussion

3.1. Operation of the annular photocatalytic reactor (APR) system

The APR system was an internally irradiated photocatalytic reactor with UV light being placed in the central core axis of the reactor. This reactor configuration resulted in minimising the stray UV light from the reactor by capturing all the photons with the stainless steel reactor core [3,21]. With such a reactor core, the net effect of the light intensity on the overall rate of photodegradation for the model compound (i.e. Congo Red) could easily be quantified [22]. Both the direct and diffuse UV light photons could be utilised in the APR system by varying the UV light configuration in the core quartz thimble [7]. Romero et al. [23] reported that the maximum effective annular radius for the utilisation of the diffuse UV photons could only occur at 5 cm from the internal reactor wall to the UV light source.

To improve the operation efficiency of the APR system in terms of its hydrodynamics, mixing and mass transfer, the TiO_2/K particles needed to be remained in homogeneous suspension by air bubbling instead of mechanical agitation. Bubble sparging with compressed air could provide a cost effective agitation and sufficient DO to prevent "electron–hole pair" recombination. However the knowledge of complete suspension of the photocatalyst particles during reactor design is essential. Two different states of suspension exist for the APR system; homogeneous suspension where the photocatalyst particles are uniformly distributed throughout the reactor and non-uniformly distributed but in complete suspension [24]. The correlation as in Eqs. (1) and (2) was proposed to predict the minimum gas velocity required for complete suspension in terms of critical TiO_2/K photocatalyst loading [24].

$$\frac{W_{\max}}{\rho_L} = 6.8 \times 10^{-4} \left(\frac{C_\mu d_T u_g \rho_G}{\mu_G}\right) \left(\frac{s_T \varepsilon_g}{u_g \mu_L}\right)^{-0.23} \left(\frac{\varepsilon_g u_{tp}}{u_g}\right)^{-0.18} \quad (1)$$

$$C_\mu = 2.3 \times 10^{-1} - 1.8 \times 10^{-1} \log \mu_L + 1.03 \times 10^{-2} (\log \mu_L)^2 \quad (2)$$

The correlation as in Eq. (1) provides a basis for reactor design, as it interrelates the important parameters such as the critical TiO_2/K photocatalyst loading (W_{max}), reactor diameter (d_T), velocity of compressed air delivered (u_g) and the gas hold-up (ε_g). The W_{max} would then be optimised in Section 3.2 and the ε_g was known to be dependent on the sparger type, solid concentration, velocity of compressed air delivered and the prevailing flow regime [25]. The dependence of ε_g on u_g is of the form of following equation [24]:

$$\varepsilon_g \sim u_g \quad (3)$$

where n is 0.4–0.7 for churn turbulent flow or transition regime and 0.7–1.2 for bubble flow regime [3,24]. With such a basis, the hydrodynamics of the APR system could be easily predicted to give a minimal operating condition.

3.2. Effects of TiO_2/K photocatalyst loading

The influences of TiO_2/K photocatalyst loading on the photodegradation rate of CR were studied in a TiO_2/K dosage range of 2–10 g/dm^3. The investigation was carried out in the APR with 40 ppm CR at natural pH. The photodegradation profiles of CR with respect to the TiO_2/K loading are shown in Fig. 2. It was observed that the photodegradation rate of CR increases with an increase in TiO_2/K loading. The degradation profile became a plateau when the TiO_2/K loading was higher than 6 g/dm^3 (Fig. 3). The reasons for the plateau in photodegradation rate at elevated TiO_2/K loading are suggested to be owing to (i) the inception of aggregation that leads to a decrease of active sites; and (ii) the increase in TiO_2/K that promotes active light scattering resulting in severe light

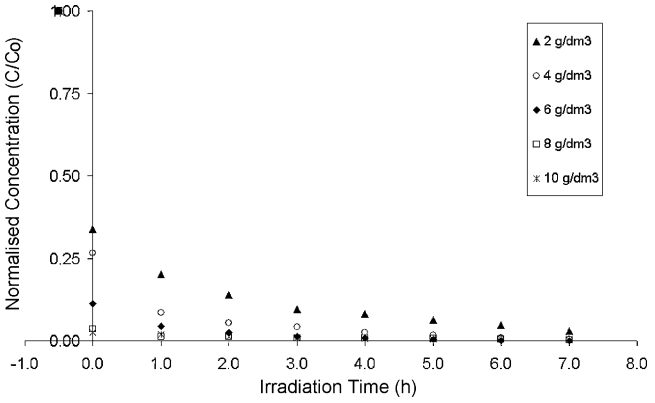

Fig. 2. Effects of TiO_2/K photocatalyst loading on CR degradation rate (pH = natural; C_0 = 40 mg/dm^3; compressed air flow rate = 10 dm^3/min). Dark adsorption start at $t = -0.5$ h. UV irradiation starts at $t = 0$ h.

attenuation through the entire reactor space [8,12,19,26]. The optimum TiO_2/K loading was found to be 6 g/dm^3. It was noted that the optimum TiO_2/K loading appeared to be much higher than for previous investigations using the commercial pure TiO_2. This is due to the weight contribution by the core kaolinite particles. From previous X-ray diffraction (XRD) study of the TiO_2/K photocatalyst, the weight ratio for the surface-attached TiO_2 crystallite to kaolinite by zinc oxide spiking method was determined to be 0.08:1.00. According to this result, it was estimated that 6 g/dm^3 of TiO_2/K may only be equivalent to 0.48 g/dm^3 of TiO_2. Some previous investigations reported that the optimum pure TiO_2 loading was in the range of 0.5–2.0 g/dm^3, depending on the reactor configuration used [27–29]. Therefore, the application of TiO_2/K with the APR system was proven to have better photo-efficiency, as it requires lower TiO_2/K loading. The degradation efficiency might be enhanced by the adsorption capability of K as the core platform, which increases the probability of surface reaction with CR. This dictates that the ultimate TiO_2/K photocatalyst should only have the 0.08 weight fraction taken into account when making direct comparison with the commercially available pure TiO_2.

3.3. Effects of initial pH

The effects of pH on photocatalytic water remediation were reported by several researchers [8,12]. Since it is impractical to maintain the pH level throughout the course of photodegradation, most of the study focussed on the simulation of initial pH for the as-received water [12]. Figs. 4 and 5 illustrate the photodegradation profiles of CR degradation in the variation of initial pH 5–12. At the initial pH ranging from 5 to 9, the photodegradation of CR was dominated by the adsorption of CR at the initial stage. The photocatalytic efficiency of the TiO_2/K was found to be inflexed at pH 9.5 as the low adsorption and photodegradation rates of CR were found to be associated with pH 10–12. This can be explained by the occurrence of point of zero charge (PZC) for the TiO_2/K photocatalyst at pH 9.5 as shown in Fig. 6. PZC is the condition where the surface charge attained by the photocatalyst particles is zero or neutral [8,12]. As

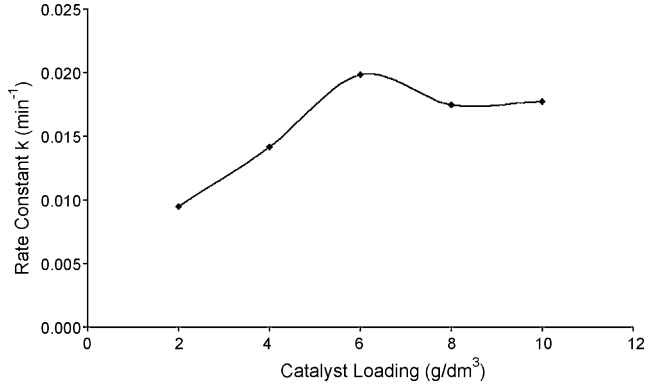

Fig. 3. Effects of TiO_2/K catalyst loading on the optimum CR degradation rate.

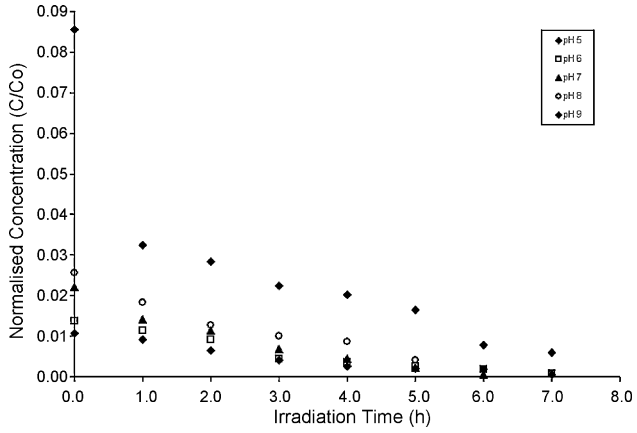

Fig. 4. The influences of different initial pH conditions (pH 5–9) on the photodegradation rate of CR. Batch operating conditions: TiO_2/K loading of 6 g/dm^3, compressed air flow rate of 10 dm^3/min and initial CR concentration of 40 ppm. UV irradiation starts at $t = 0$ h.

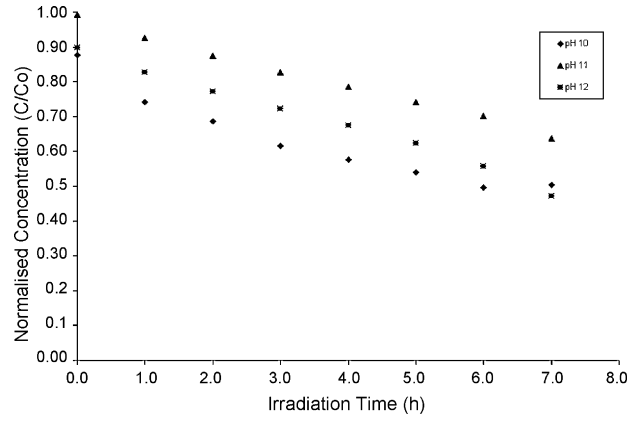

Fig. 5. The influences of different initial pH conditions (pH 10–12) on the photodegradation rate of CR. Batch operating conditions: TiO_2/K loading of 6 g/dm^3, compressed air flow rate of 10 dm^3/min and initial CR concentration of 40 ppm. UV irradiation starts at $t = 0$ h.

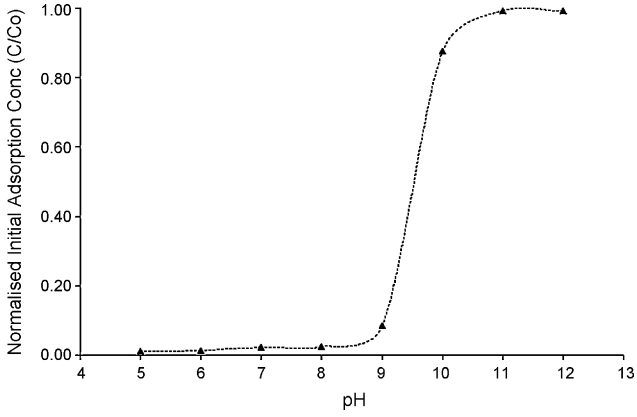

Fig. 6. Correlated plot of initial adsorption against initial solution pH for the determination of TiO_2/K surface potential.

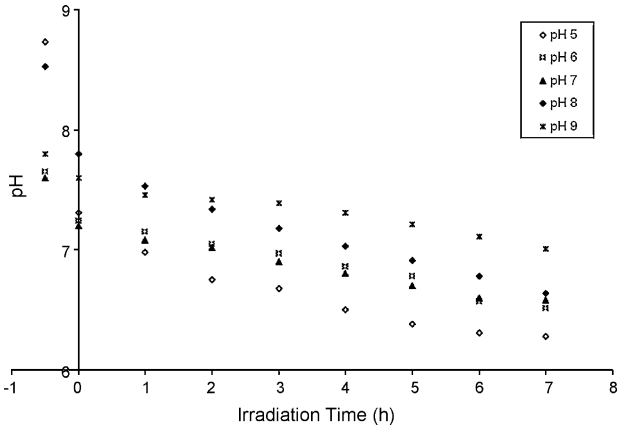

Fig. 7. The change in pH values during the photodegradation of CR for aqueous CR solution with different initial pH range of pH 5–9. Batch operating conditions: TiO_2/K loading of 6 g/dm^3, compressed air flow rate of 10 dm^3/min and initial CR concentration of 40 ppm. UV irradiation starts at $t = 0$ h.

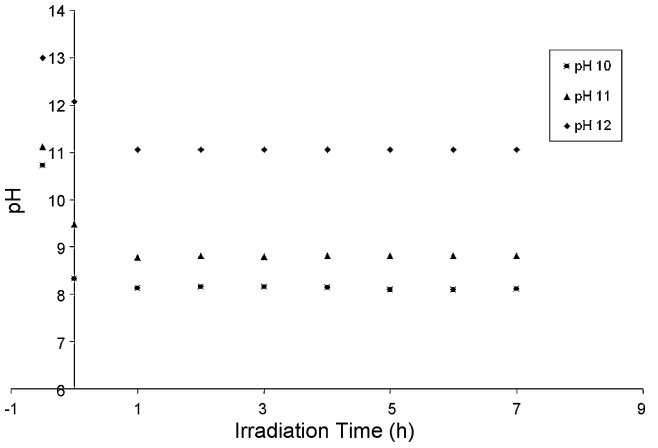

Fig. 8. The change in pH values during the photodegradation of CR for aqueous CR solution with different initial pH range of pH 10–12. Batch operating conditions: TiO_2/K loading of 6 g/dm^3, compressed air flow rate of 10 dm^3/min and initial CR concentration of 40 ppm. UV irradiation starts at $t = 0$ h.

the surface charge at pH lower than PZC, the particle surface would be positively charged while negatively charged at pH higher than the PZC [8,12]. For most TiO_2 particles, the PZC was reported to be in the range of pH 5.6–6.8 [7,8,12]. The significant deviation of the PZC for TiO_2/K over most commercial TiO_2 is proposed to be owing to either the differences in TiO_2/K preparation conditions or the ionic adsorption interaction between the TiO_2/K with the aqueous [26]. Since CR is an anionic dye, it is anticipated that the negatively charged dye molecules will have enhanced adsorption and photocatalytic reaction with TiO_2/K at a pH lower than the PZC [30].

A significant dissimilarity between the applications of commercial pure TiO_2 with the TiO_2/K particles should be noted. The TiO_2/K particles could react efficiently at a broader range of pH with further anionic molecules owing to the occurrence of its PZC at a higher pH of 9.5. This has certainly added value to the TiO_2/K photocatalyst. For instance, the TiO_2/K photocatalyst could be suitably applied to tertiary wastewater treatment since the pH of the treated water from the secondary biological treatment process was reported to fall in the range of 6.8–8.3 [26]. The use of conventional TiO_2 particles would require pH adjustment to maintain pH below pH 5.6 (i.e. nominal TiO_2 PZC) by the addition of chemicals [11]. This can generate an additional operation cost for the efficient operation of such photocatalysis process at an industrial scale.

In this study, the monitoring of pH during the photodegradation reaction was carried out. Figs. 7 and 8 show the variation in pH, corresponding to the different initial pH conditions. It could be seen that the addition of TiO_2/K has an effect on the initial pH value for the TiO_2/K/CR mixture. Fig. 7 shows that for a lower initial pH value for the aqueous CR, the resultant TiO_2/K/CR mixture would attain a pH value close to the PZC value of TiO_2/K as could be seen for initial pH 5. Subsequently the photodegradation of CR at a low initial pH (i.e. pH 5) resulted in a large change of pH range, with 2.45 drop in pH value. When the initial pH increases to 9, the photodegradation rate of CR was gradually decreased. The occurrence of PZC for TiO_2/K at 9.5 was proposed to be the main reason for the gradual decrease in the photodegradation rate. This is owing to the presence of weak electrostatic attraction force between the water molecules and TiO_2/K surface charge, which resulted in a lower generation rate of hydroxyl radicals (OH•) as justified by the small pH change at initial pH 9 [5,6]. The amount of hydroxyl radicals (OH•) generated was observed to strongly correlate to the decrease in pH (i.e. amount of H^+ concentration generated), as described by the following equation:

$$\frac{TiO_2}{K} \xrightarrow{UV} VB_{TiO_2/K} + H_2O \rightarrow {}^{\bullet}OH + H^+ \quad (4)$$

Fig. 8 shows that when the initial pH value increases to pH > PZC (TiO_2/K), the pH change during the photodegradation of CR became relatively small when UV irradiation started at $t = 0$ h. Simultaneously the photodegradation rate at pH > PZC (TiO_2/K) appeared to be impeded. Winterbottom et al. [31] proposed that this is owing to the competitive reaction of saturated hydroxyl molecules at the surface of TiO_2. The pH change might be attributed to the formation of CR associated by-products, such as the degradation products originated from the benzyl and phenyl groups of CR, and its transient formation of aliphatic acids [31,33]. Further study related to the possible formation of by-products associated with the photodegradation of CR will be discussed in Section 3.6. Since the influences of initial pH < PZC (TiO_2/K) were observed to give an analogous photodegradation rate, pH 7 was chosen for all the subsequent studies.

3.4. Effects of aeration rate

For an air-bubble agitated reactor, the knowledge of the minimal aeration rate is essential for complete suspension of the particles [12]. The Eq. (1) as given in Section 3.1 could be used to predict the minimal aeration rate required for complete suspension of TiO_2/K particles in the APR system. Prediction of the minimal aeration rate was calculated in terms of the critical TiO_2/K loading, which was 6 g/dm^3 from Section 3.2. Fig. 9 shows the predicted range of minimal aeration rate for complete suspension of TiO_2/K in the APR, in terms of different TiO_2/K loadings. Results showed that for TiO_2/K loading of 6 g/dm^3, the theoretical minimal aeration rate required was 5 dm^3/min. In the present work, the impact of the aeration rate on the photocatalysis reaction was studied by varying the aeration rate. Fig. 10 shows the photodegradation rate of CR at different aeration rate from 5 dm^3/min to 15 dm^3/min. Practically it was found that at the predicted aeration rate of 5 dm^3/min, the buoyant force provided by the air sparging was insufficient to keep the TiO_2/K in complete suspension. This could be observed from the amount of settled TiO_2/K particles on the air sparger after the study.

The results also suggested that the external mass transfer resistance exists in the APR system, as the photodegradation rate was observed to depend on the aeration rate [32,33]. A 2.5 dm^3/min step increase in the aeration rate resulted in a reduction of the external mass transfer resistance and, simultaneously increased the photodegradation rate of CR. This might be owing to the change in the

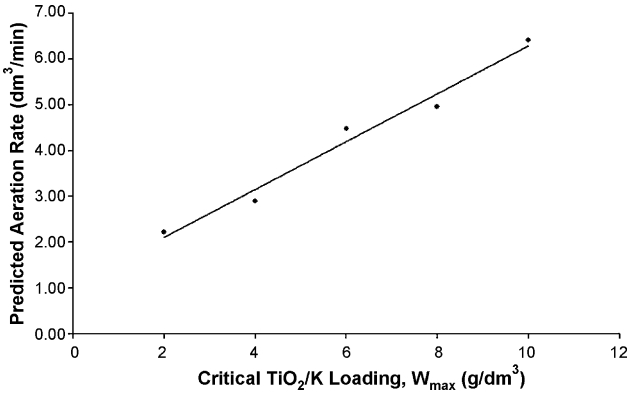

Fig. 9. Predicted minimal aeration rates required for complete suspension of TiO_2/K particles in the APR system for different TiO_2/K loading, by Eq. (1).

fluid mixing induced by the increase in both the aeration rate and dissolved oxygen to enhance the photodegradation reaction [12,33].

The dissolved oxygen in the liquid phase and the gas hold-up for the reactor need to be taken into consideration for determining the optimum aeration rate [3]. For a complete mineralisation of CR, the theoretical amount of oxygen required was determined from the stoichiometry of the balanced chemical reaction as in Eq. (5) [12]. From Eq. (5), 42.5 mol of oxygen was required for the complete degradation of 1 mol of CR.

$$C_{32}H_{22}N_6O_6S_2{}^{2-} + 2Na^+ + 42.5O_2 \rightarrow 32CO_2 + 11H_2O + 6NO_2 + 2SO_2 \quad (5)$$

Taking the operation factors of technical operability, mass transfer resistance, gas hold-up, complete suspension of TiO_2/K and dissolved oxygen into consideration, the optimum aeration rate in this study was determined to be 7.5 dm^3/min. This optimum aeration rate was found practically as a compromise of each of the factors that affects the photodegradation of CR in the APR system. When this optimised aeration rate was compared to the theoretical predicted values, it could be observed that the correlation as given by Eq. (1) was quite conservative and not well-defined for the current APR–TiO_2/K coupled system used. A correction factor of 0.4 was further required to sufficiently define this APR–TiO_2/K coupled system.

3.5. Effect of initial CR concentration

Most photocatalytic studies have reported the dependency of the reaction rate on the initial concentration of the surrogate organic substances [8,9,12]. The effects of initial CR concentration

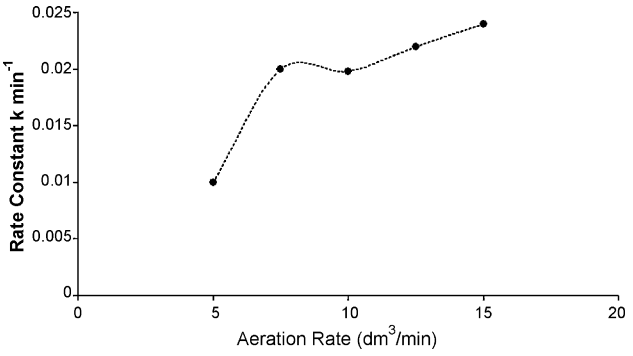

Fig. 10. Effects of different compressed air flow rate on the photodegradation rate of CR. Batch operating conditions: initial pH of 7, critical TiO_2/K loading of 6 g/dm^3, initial CR concentration of 40 ppm.

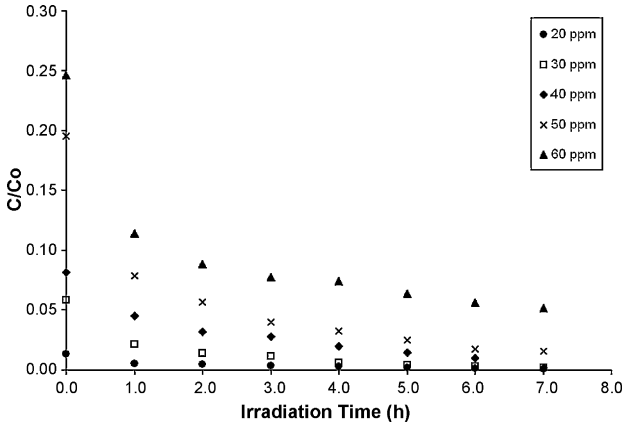

Fig. 11. Effects of different initial CR concentration on the photodegradation rate of CR. Batch operating conditions: initial pH 7, critical TiO_2/K loading of 6 g/dm^3 and compressed air flow rate of 7.5 dm^3/min.

in the range of 20–60 mg/dm^3 on the photodegradation rate were investigated under the operating conditions of pH 7, photocatalyst loading of 6 g/dm^3 and aeration rate of 7.5 dm^3/min. Fig. 11 shows the photodegradation profiles under the different initial CR concentrations. It could be observed that the increase in the CR concentration resulted in a longer irradiation time required to completely degrade the CR [30]. Such dependency was found to fit well with the zero order rate equation as given in Eq. (6) for CR concentration of up to 40 mg/dm^3. For CR concentration greater than 40 mg/dm^3, a pseudo first order rate equation was found to be the best fit. The optimum initial CR concentration, therefore, was dependent on the total amount of CR required for total conversion.

$$-\frac{dC_{CR}}{dt} = k \quad (6)$$

3.6. Mineralisation of CR and its intermediate by-products

Mineralisation refers to the complete conversion of a surrogate organic compound (i.e. CR in this study) to the innocuous final products of carbon dioxide and water. This is usually a slow reaction as it involves the formation and subsequent breakdown of intermediate by-products, as a result of the hydroxylation and rupturing of the aromatic rings [8].

In this study, the mineralisation of CR was monitored through the measurement of its corresponding COD. Since CR consists of other chemical elements such as nitrogen and sulfur, it would be inadequate to monitor the complete mineralisation process by the total organic carbon (TOC) measurements (i.e. only corresponds to the available organic carbons) [7]. Fig. 12 shows the change in COD values that correspond to the photodegradation of CR under the operating conditions of pH 7, 6 g/dm^3 of TiO_2/K loading, aeration rate of 7.5 dm^3/min and initial CR concentration of 40 ppm. During the photodegradation of CR, two ascending changes in COD values were found at 3 h and 7 h of irradiation time, respectively. This was hypothesized to be the evolvement of intermediate by-products with lower molecular weight from the rupturing and hydroxylation reaction of •OH with the principal CR structure [34–36].

Sequentially the samples collected during the mineralisation reaction were verified using the LC/MS analysis for the intermediate by-products formed. Fig. 13 shows the LC/MS analysis of CR and its intermediate by-products for irradiation time at 0 h and 7 h, respectively. The results from the MS analysis revealed that eight intermediate by-products were detected in the photodegradation solution. The resultant MS intermediate peaks were then matched with NIST and NISTREP library data and as proposed in Table 1. Table 1 lists the proposed main intermediates as identi-

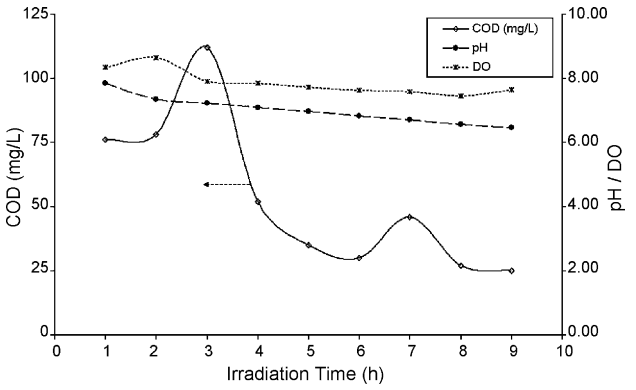

Fig. 12. Change of COD, pH and DO during the photodegradation of CR under the optimised batch operating conditions (initial pH 7; critical TiO_2/K loading = 6 g/dm^3; compressed air flowrate = 7.5 dm^3/min; initial CR concentration = 40 ppm).

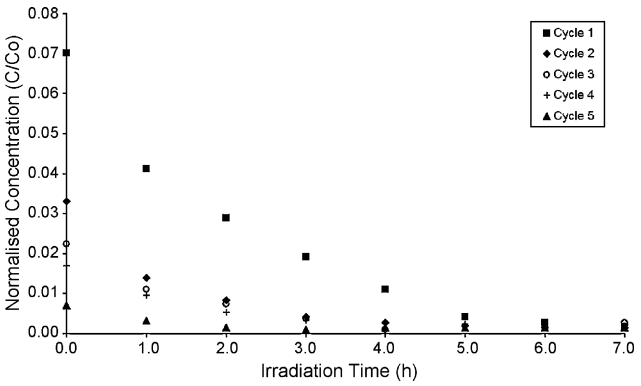

Fig. 14. Photodegradation profiles of CR for every subsequent recycle/reactivation cycle. Batch operating conditions: initial pH 7, critical TiO_2/K loading of 6 g/dm^3 and compressed air flow rate of 7.5 dm^3/min and initial CR concentration of 40 ppm.

fied in Fig. 13, their corresponding molecular weights and chemical structures.

When both the COD and LC–MS results were analysed concurrently, the two ascending changes in COD at 3 h and 7 h irradiation time could then be interrelated to the two rapid occurrence groups of MS peak at 198, 225, 248 (i.e. for 3 h) and 95, 99, 120, 130 (i.e. for 7 h). For the MS peaks group at 3 h of irradiation, most of the identified intermediate compounds contain double aromatic rings (Table 1). This indicates that the initial hydroxylation reaction of •OH attacks the azo bond (N=N) at the CR structures, resulting in the emerging of multiple chemical compounds with double aromatic bonds. For the MS peak group at 7 h of irradiation, it could be observed that the identified intermediates consist of a single aromatic ring. Although the LC analysis showed that the dominant CR peaks disappeared in 4 h, the analytical data of COD and LC/MS indicated that monitoring COD should be carried out to ensure the complete conversion of its associated intermediates. The intermediates as proposed in Table 1 provide fundamental information for the understanding of the degradation mechanisms and kinetics in the photodegradation reaction.

3.7. Comparison in photoactivity for new and reactivated TiO_2/K

Separation and reactivation of photocatalysts are one of the key issues, which make the application of TiO_2 photocatalysis for wastewater treatment technically and economically infeasible to be an industrial process [33]. Rizzo et al. [11] reported that the current technical issues include downstream separation, periodical cleaning of the catalyst surface and catalyst reactivation (i.e. particularly if the supported material cannot be calcined) that need to be considered. To date, it is known that no report on the photocatalyst reactivation has yet been reported. Most of the study was impeded by the inappropriate use of TiO_2 immobiliser to achieve constant. For instance, the use of magnetically separable ferromagnetic material or stainless steel would induce the formation of impurity phase when calcined at certain temperature [15].

In this study, the TiO_2/K photocatalyst used was separated by sedimentation followed by decantation and calcination in a furnace for catalyst reactivation. The TiO_2/K particles with average diameter of 3.5 μm promote rapid sedimentation in a settling jar. Prior to the calcination, the TiO_2/K particles were subjected to repeatedly rinsing with distilled water for three times. The

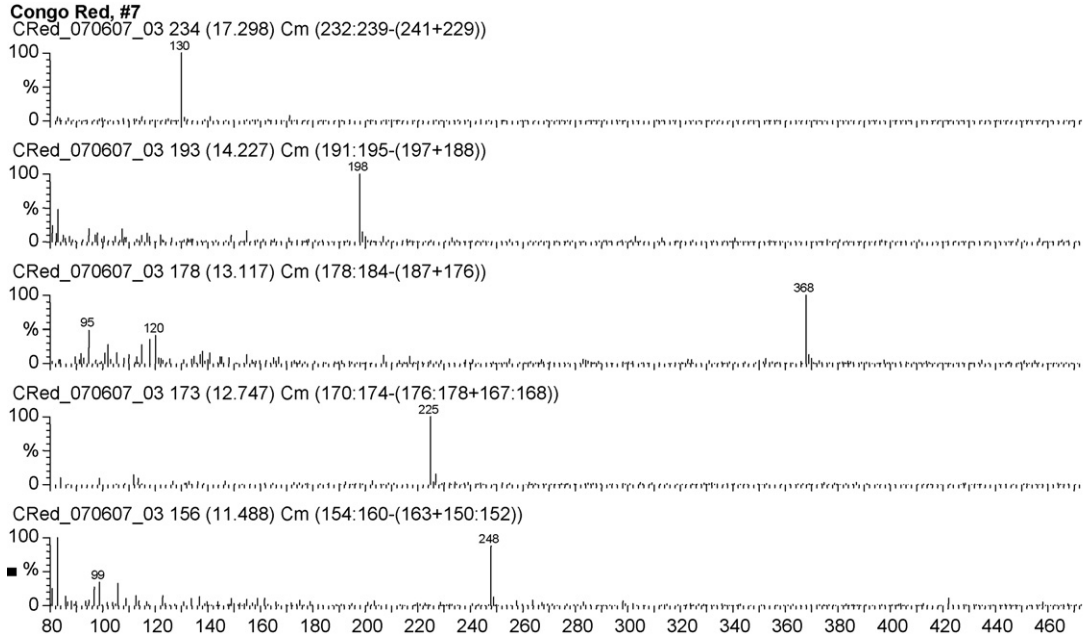

Fig. 13. LC–MS analysis of CR and its intermediate products from the photocatalytic oxidation reaction. Initial pH 7; critical TiO_2/K loading = 6 g/dm^3; compressed air flowrate = 7.5 dm^3/min; irradiation time from 0 h to 7 h.

Table 1
The intermediate compounds from the photocatalytic oxidation of Congo Red as identified by LC/MS using NIST and NISTREP library data.

Peak no.	Name of identified compound	Molecular weight *m/z*	Molecular structure
95	2(1H)-Pyridinone	95	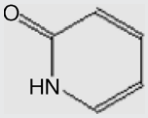
99	Piperidine, 4-methyl-	99	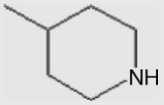
120	Benzaldehyde, 4-methyl-	120	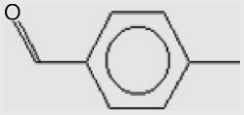
130	5-Amino-2-methoxyphenol	129	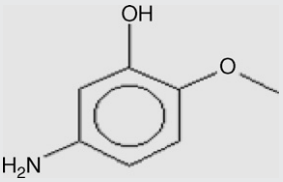
198	1,1′-Biphenyl, 4-nitro-	199	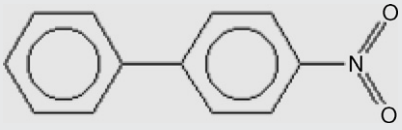
225	*p*-Anisaldehyde phenylhydrazon	226	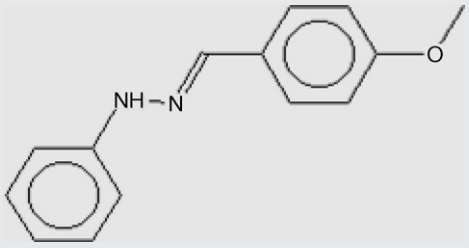
248	14 Cyclopentanecarboxamide, *n*-(2,5-dimethoxyphenyl)-	249	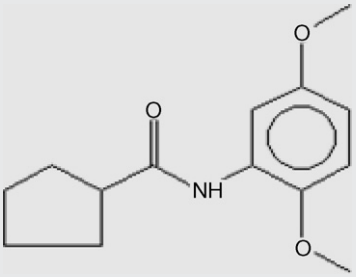
369	Diazene, bis[4-(pentyloxy)phenyl]-, 1-oxide	369	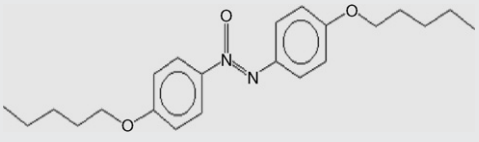

reactivation of the TiO_2/K particles was fixed at 500 °C for 10 min. Since the impurities in K were being removed during the preparation, no impurities could leach into the photocatalyst structure. Fig. 14 shows the photodegradation profile for the reactivated TiO_2/K photocatalyst under the previously optimised batch conditions. The reactivated TiO_2/K photocatalyst demonstrated a better photoactivity after each reactivation. When the TiO_2/K particles were spiked with 10 wt% of zinc oxide (ZnO) during the X-ray diffraction, it was observed that the weight ratio of TiO_2 crystalline phase to kaolinite increases from 8.0 wt% (first reactivation) to 9.0 wt% (fifth reactivation). This suggests that the reactivation temperature might affect the TiO_2 crystal growth on the incomplete amorphous–crystalline phase conversion. Therefore, further study on determining the optimum reactivation temperature and duration is necessary.

4. Conclusion

The application of the newly synthesized TiO_2/K coupled with the APR system has been demonstrated in this study. The initial pH showed a significant impact on the adsorption, in particular degra-

dation capability of the TiO_2/K particles. It was interesting to note that the PZC of TiO_2/K was pH 9.5 from the nominal PZC of pure TiO_2. This indicates that the photocatalytic reaction using TiO_2/K can take place in a broader operating pH range in the APR system. The significant hydrodynamic inputs of such a slurry APR system have also been proven, in providing a technically cost effective agitation for sufficient DO and complete suspension of TiO_2/K. The external mass transfer resistance as experienced in the APR–TiO_2/K system was found to diminish with a step increases in the aeration rate.

The experimental results also revealed that the coupled APR–TiO_2/K system is capable of high conversion of organic loading with the total conversion of CR in 4 h of irradiation and an 80% COD reduction. This was achieved under the optimal batch operating conditions of pH 7, TiO_2/K loading of 6 g/dm^3, aeration rate of 7.5 dm^3/min and initial CR concentration of 40 mg/dm^3 as obtained from the study. The possible intermediates formed during the photocatalytic degradation of CR were also proposed, as a basis for kinetic investigations towards large-scale implementation of such a coupled system. The reactivation study showed that the photocatalytic performance of TiO_2/K was enhanced diminutively for each recovery and reuse cycle up to at least 5 cycles. This showed the promising application of the APR–TiO_2/K coupled system as a tertiary wastewater treatment unit.

Acknowledgements

This work was supported by the Australian Research Council Linkage Grant (LP0562153) and Australian Water Quality Centre through the Water Environmental Biotechnology Laboratory (WEBL) at the University of Adelaide.

References

[1] R.J. Watts, S. Kong, W. Lee, Journal of Environmental Engineering 121 (10) (1995) 730–735.
[2] S.R. Couto, A. Dominguez, A. Sanroman, Chemosphere 46 (2002) 83–86.
[3] J.H. Jeon, S.D. Kim, T.H. Lim, D.H. Lee, Chemosphere 60 (2005) 1162–1168.
[4] W.L. Kostedt I.V., J. Drwiega, D.W. Mazyck, S.W. Lee, C.Y. Wu, P. Chadik, Environmental Science and Technology 39 (2005) 8052–8056.
[5] C.S. Zalazar, R.L. Romero, C.A. Martin, A.E. Cassano, Chemical Engineering Science 60 (2005) 5240–5254.
[6] C.S. Zalazar, C.A. Martin, A.E. Cassano, Chemical Engineering Science 60 (2005) 4311–4322.
[7] A.P. Toor, A. Verma, C.K. Jotshi, P.K. Bajpai, V. Singh, Dyes and Pigments 68 (2006) 53–60.
[8] I.J. Ochuma, R.P. Fishwick, J. Wood, J.M. Winterbottom, Applied Catalysis B: Environmental 73 (2007) 259–268.
[9] J.M. Herrmann, Catalysis Today 53 (1999) 115–129.
[10] I.K. Konstantinou, T.A. Albanis, Applied Catalysis B: Environmental 49 (2004) 1–14.
[11] L. Rizzo, J. Koch, V. Belgiorno, M.A. Anderson, Desalination 211 (2007) 1–9.
[12] S.S. Chin, T.M. Lim, K. Chiang, A.G. Fane, Chemical Engineering Journal 130 (2007) 53–63.
[13] R.A. Burns, J.C. Crittenden, D.W. Hand, V.H. Selzer, L.L. Sutter, S.R. Salman, Journal of Environmental Engineering 125 (1) (1999) 77–85.
[14] R.L. Pozzo, J.L. Giombi, M.A. Baltanas, A.E. Cassano, Catalysis Today 62 (2000) 175–187.
[15] Y.S. Chung, S.B. Park, D.W. Kang, Material Chemistry and Physics 86 (2004) 375–381.
[16] S. Mozia, M. Tomaszewska, A.W. Morawski, Dyes and Pigments 75 (2007) 60–66.
[17] N.J. Peill, M.R. Hoffmann, Environmental Science and Technology 32 (1998) 398–404.
[18] S.B. Kim, S.C. Hong, Applied Catalysis B: Environmental 35 (2002) 306–315.
[19] A. Bhargava, M.F. Kabir, E. Vaisman, C.H. Langford, A. Kantzas, Industrial, Engineering Chemistry Research 43 (2004) 980–989.
[20] M.N. Chong, V. Vimonses, S. Lei, B. Jin, C. Saint, C. Chow, Microporous and Mesoporous Materials 117 (2009) 233–242.
[21] M.F. Kabir, E. Vaisman, C.H. Langford, A. Kantzas, Chemical Engineering Journal 118 (2006) 207–212.
[22] A.V. Emeline, X. Zhang, M. Jin, T. Murakami, A. Fujishima, Journal of Physical Chemistry B 110 (2006) 7409–7413.
[23] R.L. Romero, O.M. Alfano, A.E. Cassano, Industrial Engineering and Chemical Research 36 (1997) 3094–3109.
[24] R.V. Chaudhari, Y.T. Shah, in: S. Whitaker, A.E. Cassano (Eds.), Concepts and Design of Chemical Reactors, vol. 3, Gordon and Breach Science Publishers, New York, 1986, pp. 243–298.
[25] B. Jin, P. Lant, Chemical Engineering Science 59 (2004) 2379–2388.
[26] R.L. Pozzo, J.L. Giombi, M.A. Baltanas, A.E. Cassano, Applied Catalysis B: Environmental 38 (2002) 61–69.
[27] A. Mills, S. Morris, Journal of Photochemistry and Photobiology A: Chemistry 71 (1993) 75–83.
[28] D. Chen, A.K. Ray, Water Research 32 (1998) 3223–3234.
[29] A. Bhattacharyya, S. Kawi, M.B. Ray, Catalysis Today 98 (2004) 431–439.
[30] S. Erdemoglu, S.K. Aksu, F. Sayilkan, B. Izgi, M. Asilturk, H. Sayilkan, F. Frimmel, S. Gucer, Journal of Hazardous Materials (2007) 087, doi:10:1016/j.jhazmat.2007.11.
[31] J.M. Winterbottom, Z. Khan, A.P. Boyes, S. Raymahasay, Environmental Progress 16 (1997) 125–131.
[32] P.F. Biard, A. Bouzaza, D. Wolbert, Environmental Science and Technology 41 (2007) 2908–2914.
[33] S. Mozia, M. Toyoda, M. Inagaki, B. Tryba, A.W. Morawski, Journal of Hazardous Materials 140 (2007) 369–375.
[34] K. Tanaka, K. Padermpole, T. Hisanaga, Water Research 34 (2000) 327.
[35] Y. Xu, C.H. Langford, Langmuir 17 (2001) 897.
[36] C. Guillard, H. Lachheb, A. Houas, M. Ksibi, E. Elaloui, J.M. Hermann, Journal of Photochemistry and Photobiology A: Chemistry 158 (2003) 27.